GRAIN MAPPING BY DIFFRACTION CONTRAST TOMOGRAPHY: EXTENDING THE TECHNIQUE TO SUB-GRAIN INFORMATION

A. King, P. Reischig, Simon Martin, Joao F. B. D. Fonseca, M. Preuss, Wolfgang Ludwig

GRAIN MAPPING BY DIFFRACTION CONTRAST TOMOGRAPHY: EXTENDING THE TECHNIQUE TO SUB-GRAIN INFORMATION

Andrew King
Peter Reischig[1-3], S. Martin[3,4], J. Fonseca[4], M. Preuss[4] ,W Ludwig[3,5]

GKSS research centre, Germany
[1]Institute for Syncrotron Radiation, Karlsruhe Institute of Technology, Germany
[2]Delft University of Technology, Delft, Netherlands
[3]ESRF, Grenoble, France
[4]Materials Science Centre, Manchester University, UK
[5]MATEIS, INSA de Lyon, Villeurbanne, France

ABSTRACT

During the last few years diffraction contrast tomography has become established as a technique for mapping polycrystalline microstructures in 3D. The experiment combines aspects of synchrotron microtomography and of 3D-XRD. The diffraction spots arising from individual grains are recorded with high spatial and angular resolution, and reveal evidence of sub-grain structures. However, the interpretation and exploitation of this information is not simple. The present manuscript will describe diffraction contrast tomography, and show examples of the data collected. Two concepts for the interpretation of the data will be described. Some preliminary results of a study of the in-situ deformation of polycrystalline aluminium will be shown. However, the aim of this paper is to show examples of the data available, and to enable an open discussion of possible techniques for its analysis. Perspectives will be given for future grain tracking experiments at the newly commissioned high energy materials science beamline at Petra III, Hamburg.

1. INTRODUCTION

Most engineering materials are polycrystalline. This means that they are composed of an aggregate of crystallites, known as grains. These crystallites have anisotropic bulk and surface properties, and therefore the behaviour of the aggregate is determined by the interactions between these grains (Sylwestrowicz and Hall 1951; Wright and Field 1998). To understand a range of physical or chemical phenomena it is necessary to know the grain structure of materials in 3D. For a complete understanding, it is necessary to map grain shapes, positions, elastic

strains and orientations. Furthermore, this should be done non-destructively, so that the characterisation can be combined with other techniques, or used to follow processes *in-situ*.

One field of research that requires this type of information is the study of plasticity in polycrystalline materials. The anisotropic properties of the grains mean that when a material is loaded, some deform plastically before others. Combined with the requirement that the grains deform cooperatively, maintaining continuity at the grain boundaries, this means that deformation is not uniform. Local concentrations of plastic strain can result in microstuctural damage, or crack initiation, and so the understanding of this behaviour is of great interest for the design and lifing of new structural materials and the development of appropriate microstructures. As a result of inhomogenous plastic deformation initially undeformed grains will develop misorientated sub grains, referred to as mosaicity. Polycrystalline deformation can be modelled using continuum crystal plasticity models (Fonseca, Oliver, Bate and Withers 2006). These models have progressed in sophistication beyond the point where their predictions can be verified using conventional experimental techniques. Further improvements of these models require new experimental techniques that can quantify the progress of deformation in 3D, non-destructively and *in-situ*.

2. CURRENT TECHNIQUES

Currently available laboratory techniques such as EBSD provide 2D information from surfaces, but bulk information is unavailable unless destructive sectioning techniques are employed (Dingley and Randle 1992). However, several techniques now exist for mapping grain shapes and orientations in polycrystalline microstructures non-destructively. The two principle approaches are polychromatic X-ray Laue-microdiffraction and its extension into 3D via differential aperture x-ray microscopy (Larson, Yang, Ice, Budai and Tischler 2002), and monochromatic beam X-ray diffraction techniques such as 3D X-ray diffraction microscopy (3DXRD) and X-ray diffraction contrast tomography (DCT) (Poulsen 2004; Ludwig, Schmidt, Lauridsen and Poulsen 2008; Johnson, King, Honnicke, Marrow and Ludwig 2008). This article will focus on this second family of techniques, which use the diffraction of synchrotron radiation to determine grain shapes, positions, and crystallographic orientations. Many features of the DCT and 3DXRD techniques are very similar. This article will focus on DCT, which is characterised by near-field imaging with an open (non-focused) beam, but many of the observations and ideas are equally applicable to 3DXRD. The basic experimental setup used for DCT is shown in figure 1(a), and the technique is described in section 4.

Two further techniques provide a more detailed insight into the processes taking place within a single grain. Topotomography involves aligning a single grain with a scattering vector parallel to the axis of a rotation stage (Ludwig, Cloetens, Härtwig, Baruchel, Hamelin and Bastie 2001). The grain can then be rotated, and a series of diffraction spot images acquired at evenly spaced rotation increments for reconstruction of the grain shape by a modified fan beam tomography algorithm. In the case of a nearly perfect crystal, distortions in the crystal lattice change the Bragg reflectivity, and this quantity is reconstructed in 3D within the grain volume.

For larger degrees of deformation, high resolution 3D-XRD provides a means of studying dynamic processes within a single grain (Jakobsen, Poulsen, Lienert and Pantleon 2007). The technique involves illuminating a sample with a low divergence, low bandwidth synchrotron beam, and imaging a single diffraction spot with a 2D detector at long distance from the sample, such that the effect of the grain size on the diffraction image is negligible (grain size ~ pixel size). By rocking the sample, 3D reciprocal space maps of the diffraction spot can be constructed, with sufficient angular resolution to distinguish sub-grains or deformation

structures within the grain. Combined with in-situ deformation, the development of these deformation structures and the associated local elastic strains can be investigated. The disadvantage of the technique is that the spatial distribution of the deformation structures within the grain is not known. Furthermore, unless the technique is combined with characterising the sample by 3D-XRD or DCT, the grain orientation, shape, and neighbourhood remain unknown.

3. CURRENT STATE OF THE ART

Studying deformed or deforming polycrystalline materials is therefore a challenging project, but one which is of potentially great interest. There is a need for a technique that allows deformation substructures to be characterised, non-destructively and in 3D, in all grains of a polycrystalline sample. This technique could be supplemented by the techniques described above which provide detailed insights into single grains, or used to identify interesting grains which could then be further investigated.

Perhaps the most promising results to date for mapping deformed polycrystalline microstructures have been published by West, Schmidt, Sørensen, Winther, Poulsen, Margulies, Grundlach and Juul Jensen (2009). Here several 2D slices through a sample of 30% deformed aluminium were reconstructed based on 3D-XRD data, but using a novel, undescribed algorithm. These maps have a spatial resolution of around 10 microns, and the sample contained about 10 grains, of which about six are visible in each reconstructed slice. The degree of deformation is much greater than has previously been dealt with using such methods.

This paper will describe efforts to map deformation processes and structures by extending the technique of diffraction contrast tomography. The aim is to study the onset of plasticity (the first few percent of plastic deformation), where the degree of mosaicity within grains is relatively small. In this regime the deformations within the grains results in distortions of the recorded diffraction spots. The aim of the work is to interpret these distortions so as to reveal the underlying deformation. First, the basic technique of diffraction contrast tomography will be described, followed by the changes implemented to study plasticity. The algorithms used to interpret the data will be discussed briefly, and preliminary results will be presented,

4. DIFFRACTION CONTRAST TOMOGRAPHY

Diffraction contrast tomography is a synchrotron x-ray diffraction imaging technique for mapping grain shapes and orientations in polycrystalline materials (Ludwig et al 2008, Johnson et al 2008). The basic experimental setup is shown in figure 1(a). The equipment used is essentially the same as is used for regular synchrotron x-ray tomography. The sample is mounted on a precision rotation stage, and illuminated by a monochromatic beam ($\Delta E/E \sim 10^{-3}$-10^{-4}). A 2D detector is positioned just after the sample, with a field of view large enough to capture both the radiograph of the sample, but also diffraction spots arising from grains within the sample as it rotates and they pass through diffracting alignments. The sample is rotated through 360º, and images are integrated over small angular increments, typically 0.05-0.1º.

Data processing of the images consists of subtracting background intensities, with the aim of leaving only contrasts due to diffraction, or extinction in the direct beam region. The diffraction spots are then segmented from the images, and data describing the spots stored in a database for further processing. If the diffracted intensity of a spot extends to more than one image, the consecutive images are summed together. Diffraction vectors associated with the diffraction spots are determined by finding Friedel pairs. These are pairs of diffraction spots occurring 180º apart during the scan, arising from the (hkl) and $(\bar{h}\bar{k}\bar{l})$ scattering vectors from the same grain.

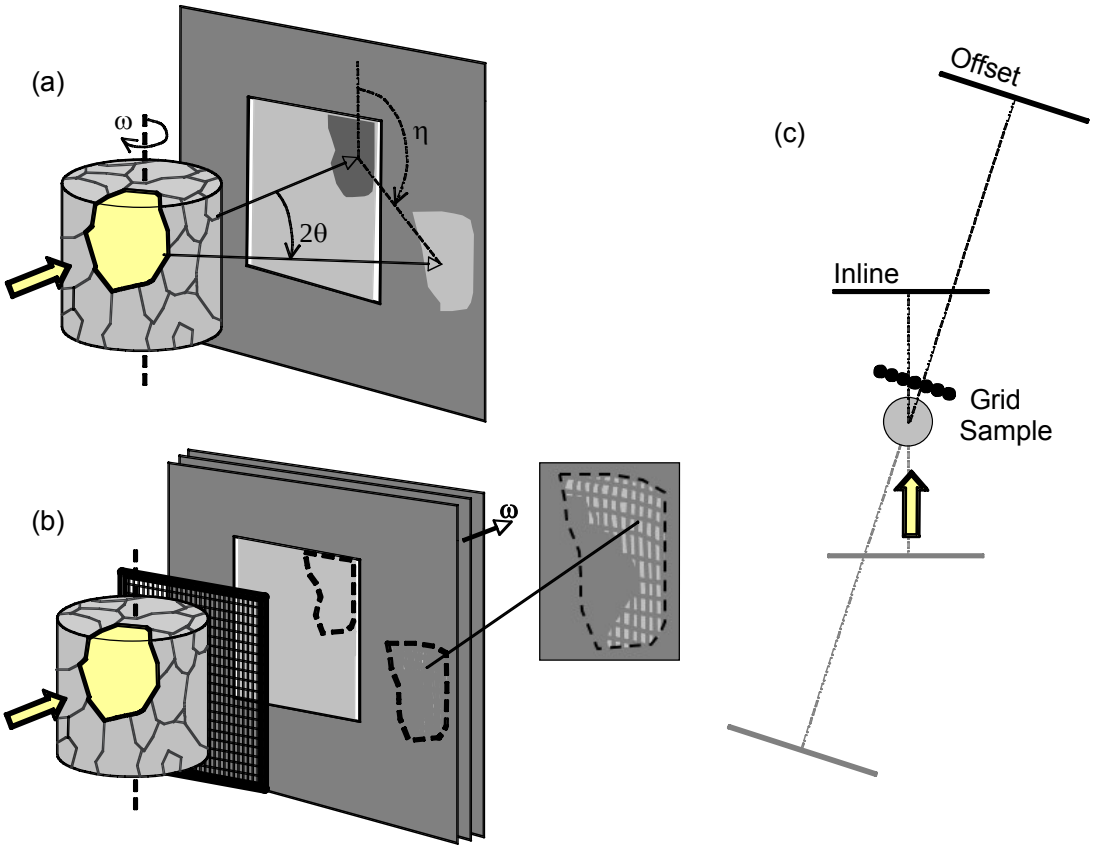

Fig. 1 (a) Standard DCT setup. (b) Combined DCT and reticulography concept. (c) Plan view of the two detector positions used. In grey the 180º "virtual detector".

Using this construction the diffraction angles 2θ, η and ω associated with the pair, and also the path of the diffracted beam through the sample, can be determined precisely (Ludwig, Reischig, King, Herbig, Lauridsen, Johnson, Marrow and Buffière 2009). The angles are defined in figure 1(a).

This is followed by an indexing operation to assign pairs of spots, as well as any remaining unpaired spots, to the grains from which they arise. The position of the grain in the sample and its crystallographic orientation are determined in this step. Finally, the grain shape is reconstructed based on a 3D ART reconstruction algorithm. The grain map is assembled from the individual grain reconstructions. Any disputed or unassigned voxels in the grain map are filled by postprocessing morphological dilation.

The radiographs acquired on the central part of the detector can be used to reconstruct the sample volume via conventional filtered backprojection, revealing any features within the sample visible in absorption contrast, as well as the precise external shape of the sample. This shape can be used as a mask to define the exterior of the grain map.

4.1 Extension to subgrain mapping. The DCT methodology described results in a map in which the shape and the crystallographic orientation of grains are known. Although this average orientation is precisely determined, only a single value is available to describe the grain. Some idea of the degree of mosaicity within a grain can be derived from the observed spreading of the diffraction spots assigned to a grain in omega, the scanning angle. A grain containing a larger degree of misorientation can be expected to spread over several images, as different parts of the

grain diffract at slightly different alignments. Additionally, the spot shape will be distorted from the ideal parallel projection of the grain volume. Both these effects are observed during scans. It should be noted that, in the same way that a single diffraction spot is insufficient to determine the orientation of a grain, a single diffraction spot cannot reveal all information about the misorientations inside a grain.

The idea developed in this paper is to first reconstruct the grain shapes and average orientations for all grains in a sample, to provide a basic grain map. Then a more detailed analysis of the distortions seen in the diffraction spots will be used to analyse sub grain misorientations, or deviations from the average grain orientation. Two ideas have been tested; one based on reticulography (Lang and Makepeace 1996), and one based on a linear least squares analysis of the images.

4.2 Reticulography. Reticulography is a topography technique developed by Lang and Makepeace for analysing misorientations in single crystals (Lang and Makepeace 1996). Topography is the imaging of a sample using radiation diffracted from the sample. In reticulography, an x-ray absorbing grid structure is placed between the sample and the detector, close to the sample. Distortions in the crystal lattice result in variations in the directions of the diffracted beams from the sample. These distort the image of the grid on the detector. By analysing these distortions, the misorientations in the crystal can be determined quantitatively. As described in Lang and Makepeace (1996), only one diffraction spot is used, so not all components of the misorientation can be analysed.

To combine reticulography and DCT, an absorbing grid was placed just after the sample, as shown in figure 1(b). The idea is that in each diffraction spot, the distorted grid image would reveal the distribution of local diffraction angles. By combining the information from multiple projections per grain, a reconstruction or fitting procedure can be used to determine the distribution of orientations within the grain.

The sample to detector distance was increased to provide a longer distance between the grid and the detector, to increase the sensitivity of the system to small misorientations. Increasing the sample-detector distance reduces the solid angle covered by the detector. To best use the reduced solid angle, the detector was rotated by 18° around the position of the rotation axis with respect to the direct beam, and so centred on the position of the {220} and {311} diffraction spots, as shown schematically in figure 1(c). As shown in figure 1(c), this geometry still allows diffraction spots to be analysed in terms of Friedel pairs using the construction described in Ludwig et al (2009), but less diffraction spots are recorded. Tilting the detector has the additional advantage of keeping the diffracted beams closer to normal incidence on the detector, thus reducing the parallax effect. This allows a thicker, more efficient scintillator to be used with less cost to detector resolution. In this configuration the direct beam and absorption/extinction images are not recorded. The grain map can still be reconstructed from the diffraction spots. In practice, scans were performed in both the conventional, in-line geometry, and the tilted geometry, so the grain map could be reconstructed from the in-line scan, with the benefit of more diffraction spots per grain, and spots which are closer to the parallel projection assumed by the ART reconstruction.

4.3 Linear approach. A second approach for the analysis of misorientations was developed which does not require the absorbing grid structure. In this approach, each grain is subdivided into a number of smaller elements. A forward projection algorithm is used to predict the diffraction spots that would be expected based on the grain shape. The observed diffraction spots are compared with the predictions, and the differences used to adjust the distortion of each

element, based on a linearised model of the diffraction geometry. The forward simulation is then repeated, and the results again compared to the observed diffraction spots. The process is repeated iteratively until convergence. The process has the advantage of simplicity, as no additional equipment or changes to the scanning methodology are required. Furthermore, the linearised approach is computationally efficient. The linear model and the algorithm have been developed by Peter Reischig, and will be further described elsewhere (Reischig 2010).

Datasets have been acquired for analysis in both the conventional, in-line geometry, and also in the offset, tilted detector geometry described above. Because this method is still in development, it is as yet undetermined which geometry provides the optimum results. The results shown are based on a preliminary analysis of part of the recorded data. They are not intended as a finished study, but rather to illustrate the concepts and ideas behind the work for the purposes of discussion. Further work will involve gaining experience with the computational tools to obtain the best possible results, completing the analysis for all data acquired, and comparison with the results of modelling work.

5. EXPERIMENTAL RESULTS

The misorientation mapping approaches described above were tested at beamline ID11 of the ESRF during experiment MA752. The sample studied was a pure aluminium cylinder, 1 mm in diameter and 1.5 mm long. Pure aluminium was chosen for its low yield stress so that diffraction spot distortions due to elastic strains would be minimised. The sample was produced by electro-discharge machining from a plate that had been heat treated to give a large grain size with as little lattice distortion as possible. The sample was mounted in a miniature in-situ loading device. The experimental apparatus was installed on top of a diffractometer, which allowed the entire assembly to be rotated around a vertical axis to obtain the tilted, offset geometry. Scans were recorded in both in-line and offset geometries, with and without the reticulography grid structure, with in-situ compression of the sample between scans. For an initial, unloaded state, compression was continued into plasticity (~37 MPa applied stress). The sample was illuminated with a 30 keV monochromatic x-ray beam ($\Delta E/E$ ~10-3) from a double Si crystal Laue monochromator. In all cases, a FReLoN camera with a scintillator and visible light microscope optic was used giving an effective pixel size of 3 microns, and hence a field of view of 6 mm from the 2k x 2k detector pixel array (Labiche, Mathon, Pascarelli, Newton,

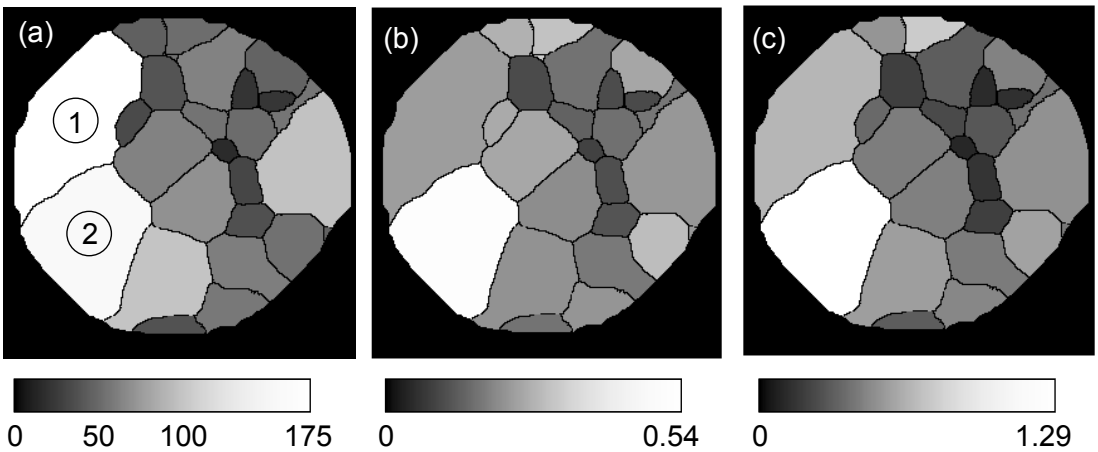

Fig. 2 DCT reconstruction. Coloured by (a) grain radius /microns (calculated from volume, noted many of these grains are cut by edge of gauge volume). (b) Mosaicity determined from extent of diffraction spots in ω (10-90th percentile) /degrees. (c) Mosaicity from total ω extent/degrees.

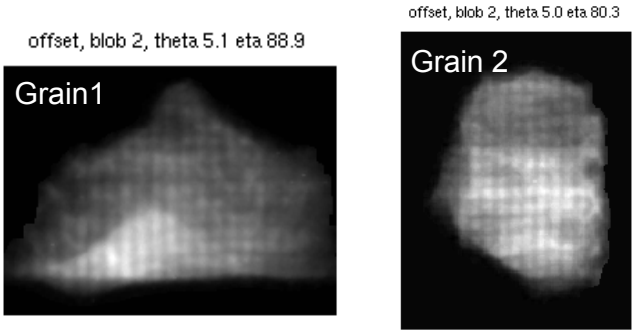

Fig. 3. Selected diffraction spots in which the absorbing grid structure is visible.

Ferre, Curfs, Vaughan, Homs and Carreiras 2007). In-line scans were performed at a sample-detector distance of ~5.75 mm, while offset scans were performed at ~13 mm, with an angular offset of 18°, corresponding to the {220} and {311} diffraction spots. The η (azimuthal) angle covered was approximately 90°, from 45-135°. This offset geometry accessed approximately half the number of spot pairs that were visible in the in-line scans.

5.1 DCT reconstruction. Figure 2(a) shows a section through the grain map of the sample determined from the initial in-line scan. 126 grains have been reconstructed in this volume. The average grain diameter is ~200 microns. Some cube type texture is observed. Two of the largest grains visible in figure 2(a) have been labelled as grains 1 and 2. Diffraction spots from these grains will be used as examples.

5.2 Images of spots with the grid. Figure 3 shows diffraction spot images from the two large grains in which the absorbing grid structure is visible. However, in many cases, the grid structure is not visible in the diffraction image, or the contrast is too poor to be exploited. This is due to a number of problems. One is that the grid structure used was not sufficiently absorbing at the x-ray energy used. Furthermore, it seems that large variations in the η angle within a diffraction spot blur the grid image in that direction. The spots shown are from {111} reflections, where the small 2θ angle means that sensitivity to variation in η is minimum. In spots with η close to 90º or 270º, as in these examples, the vertical lines of the grid are typically more visible than the horizontal lines. The vertical direction is closer to the circumferential to the direct beam, and so vertical features are not blurred by η variations. Variations in 2θ, which would tend to blur the vertical lines are much smaller because the rather soft material does not support large elastic strains.

For this sample, no further analysis was performed due the lack of useful contrasts. However, the concept of DCT combined with reticulography may be useful for studying materials in which the mosaicity is lower.

5.3 Effect of detector position. Diffraction spots corresponding to the same scattering vectors in the two experimental geometries are shown for grain 1 in figure 4. Two spots, approximately 90º apart in ω are shown. These spots are produced by summing the intensities in several consecutive images. The absorbing grid structure can be is visible in some of the spot images for the offset scan. The extra distortion in the spots recorded at the longer working distance is clearly visible. The figure shows Friedel pairs of spots. The diffraction spot shape predicted based on the reconstructed grain shape and assuming parallel projection geometry is shown in each case for comparison. The undistorted shape is "in between" the two distorted spot shapes. Certain features of the distortion can be identified as anti symmetrical between the paired spots.

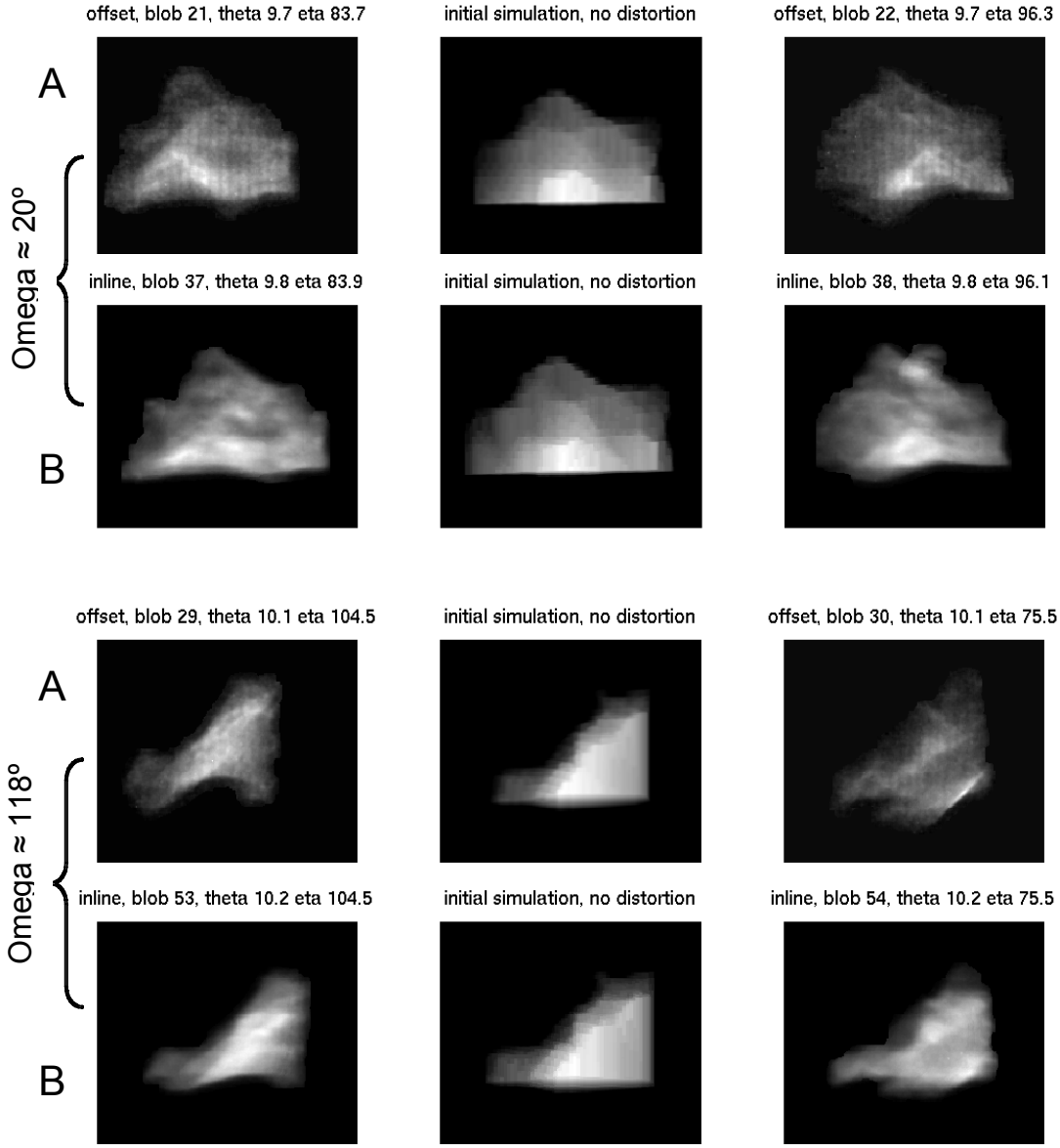

Fig. 4. Effect of detector position on diffraction spots from grain 1. Rows marked "A": 13.1 mm working distance, detector tilted by 18°. Rows marked "B": 5.75 mm, detector normal to synchrotron beam. The simulated diffraction spot assuming a parallel projection is shown in the centre.

These images demonstrate that the reconstruction of grain shapes based on the use of diffraction spots as grain projections is limited by the extent of these distortions. It appears that to improve on the current accuracy of grain reconstructions will require a new approach that takes sub grain misorientations into account.

The distribution of the diffracted intensity within a spot that is observed in the scanning direction, ω, is shown in figure 5.

5.4 Quantifying mosaicity. It is possible to obtain a crude measure of the mosaicity in a grain from the ω extension of the diffraction spots of the grain during the scan. Assuming monochromatic plane wave illumination and neglecting dispersion effects, the diffraction spots of a perfect grain will appear in a single image only, as the whole volume of the grain will be aligned for diffraction at a single rotation position of the sample. A grain containing a spread of

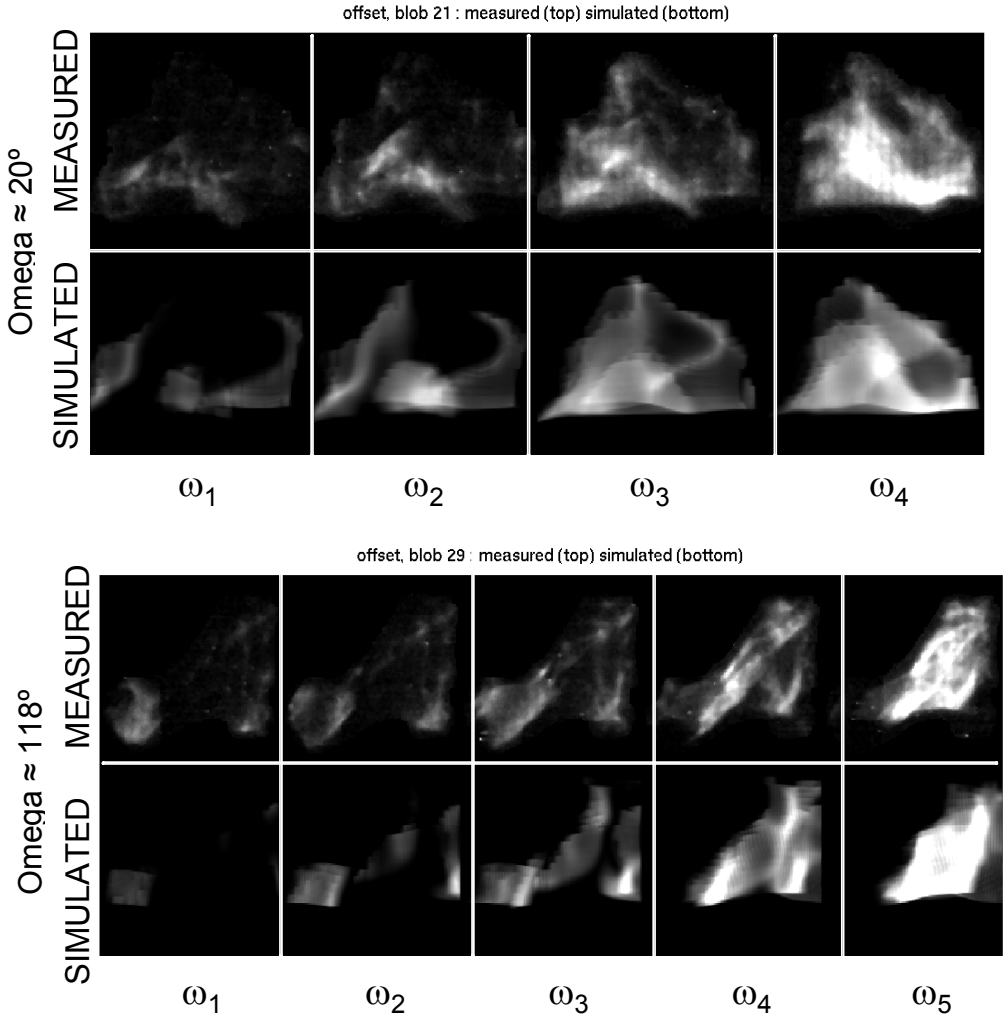

Fig. 5. Spread of diffraction spots across multiple omega images (0.1º / image) for grain 1. Note this is not the full extent of the omega extent, as only images containing significant intensity are shown. Measured and simulated intensities.

orientations will diffract over several images as different parts of the grain diffract at slightly different omega positions.

The observed extension of diffraction spots can be related to the range of orientations present in the grain. The ω range of a diffraction spot is the result of several factors. These include the bandwidth of the incident radiation, dispersion effects arising from the diffraction geometry, the Darwin width of the reflection, and the orientation spread. The shift in diffraction angles induced by the finite bandwidth ($\Delta E/E=10^{-3}$) and dispersion effects are small compared to the ω scanning increment of 0.1°. The Darwin widths of the observed reflections, for a perfect aluminium crystal at 30 keV, are of the order of 10^{-4} º-10^{-5} º, and therefore negligible.

A geometric factor (the Lorentz factor) must also be considered. Scattering vectors lying close to the rotation axis (η close to 0° or 180°) pass more slowly through the Bragg condition than those perpendicular to the rotation axis (η ~ 90° or 270°). The observations have been corrected for this geometric effect.

It should be noted that not all components of distortion will change the ω position of a single reflection. Therefore, the ω ranges associated with all spots assigned to a grain have been measured, and the mean value used to quantify the mosaicity. The quantity used is the total ω

range after correction for the Lorenz factor. However, it should be further noted that all components of distortion (elastic and plastic) *can* effect the ω position at which diffraction is observed. Therefore it is in principle possible to determine the complete orientation and strain tensor of a grain, or element of a grain, using only observations of the ω positions of diffraction events.

Figures 2(b) and 2(c) shows sections through the grain map coloured according to this measure of mosaicity. The data are taken from the inline scan, for the sample in the as received, nominally undeformed state. It can be seen that a large variation in the initial mosaicity is visible. The spread in the data is between approximately 0.3º and 1.3º if the maximum spread within each grain is calculated. The ω extent between the 10th and 90th percentiles of intensity in each spot is also recorded, and this value gives a range of roughly half the mosaicity of the maximum spread figure.

In most cases, grain size correlates well with mosaicity. Figure 6 shows mosaicity plotted as a function of grain radius for all grains, and for bulk grains only. This suggests that in this sample, which was prepared by electro discharge machining, the surface grains are not significantly more deformed than the bulk grains.

5.5 Linear algorithm results. The iterative algorithm described above has been applied to six grains which intersect the slice through the sample shown in figure 2. The algorithm has been used separately on the datasets recorded using the inline and offset detector geometries. The code allows nine distortion components to be determined - the six components of the elastic strain tensor, and three components of rotation. For the pure aluminium sample studied, the magnitudes of the elastic strains were assumed to be negligible compared to the rotations, and so only the rotations were calculated.

The simulated distorted diffraction spots resulting from the algorithm are shown in figure 7, compared to the observed spots and the initial, undistorted simulated spots. Figure 5 also shows the how the

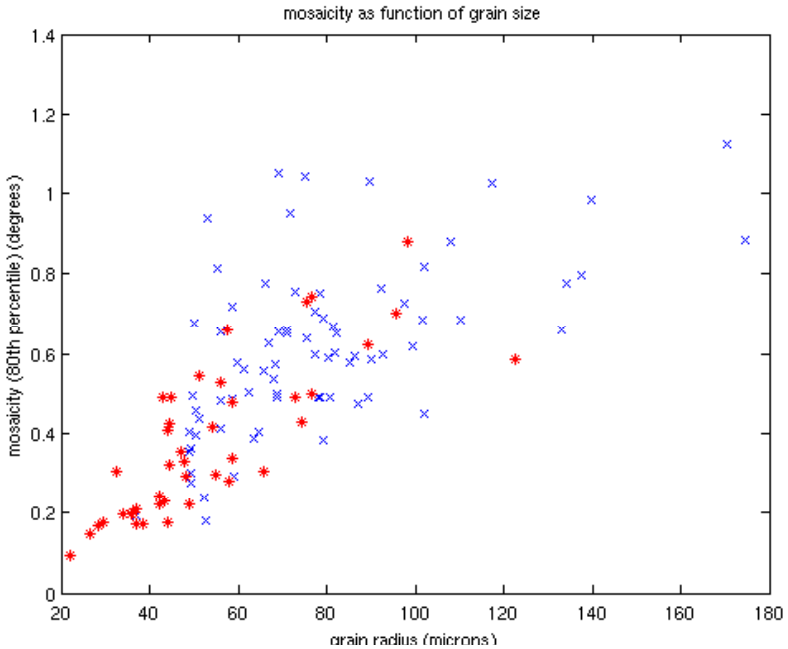

Fig. 6. Grain mosaicity (determined from the 10-90th percentile spot ω range) as a function of grain radius. Red points are bulk grains, others are surface connected.

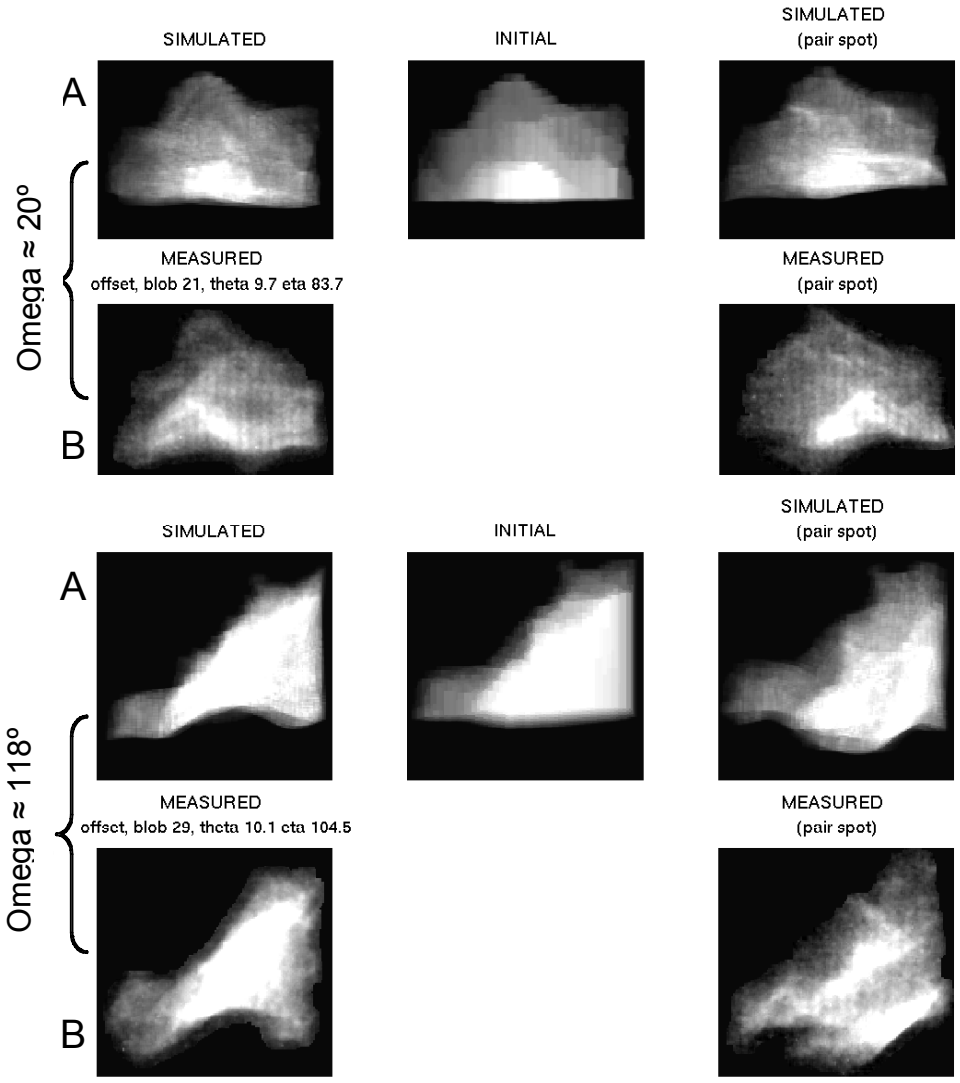

Fig. 7. Comparison of simulated (A) and measured (B) diffraction spots from grain 1. Top {311}, spot width ~500 μm. Bottom {222}, spot width ~350. μm.

intensity of simulated spots is distributed in ω. It can be seen that the simulation reproduces many of the features of the observed spots.

Figures 8 and 9 show the misorientation maps determined from the two datasets for the same section through the sample. The figures show the three components of misorientation that were determined, an image in which the three misorientations were used to determine the three components of an RGB colour.

5.6 Comparison of the two datasets. Comparing figures 8 and 9 it can be seen that some, but not all, features of the misorientation distribution are reproduced by the analysis of the two scans. The sample is in the same condition in the two scans, only the experimental geometry has changed. Therefore the misorientations calculated should be the same. In this example, for grains where a large number of diffraction spots are available, only the diffraction spots common to the two scans have been used for the analysis. Differences may arise due to different parameters used in segmenting the diffraction spots in the two scans. It is also possible that the grid structure has an adverse effect. It remains to be seen which detector geometry produces the more reliable results. A further possibility would be to combine the data from the

two detector positions to increase the number of observations. This would be a natural extension of using a 3D detector system where two working distances are available simultaneously (Olsen, Schmidt and Poulsen 2008).

5.7 Comparison with average mosaicity values. A comparison can be made between the average mosaicity values determined from the extension of diffraction spots in ω, and the spread in orientation values calculated by the linear algorithm. These results are plotted, for the two datasets, in figure 10, and show reasonable correlation between the two measures.

6. DISCUSSION

The results presented clearly show the effect of grain distortions or mosaicity on the diffraction spots observed. Two approaches for analysing such images in a quantitative way have been proposed, and the results of some initial tests presented. However, before these ideas can be used with confidence, a number of issues need to be addressed.

6.1 Validation. The most important requirement is that the results of the linear algorithm are verified by another technique. A possible approach could be the use of EBSD, or high angular resolution EBSD, on the surface of a sample, or a section through a sample (Wilkinson, Meaden and Dingley 2006). In the case of sectioning a sample it is important that no additional distortion is introduced by cutting. Alternatively, 3DXRD measurements made in new scanning

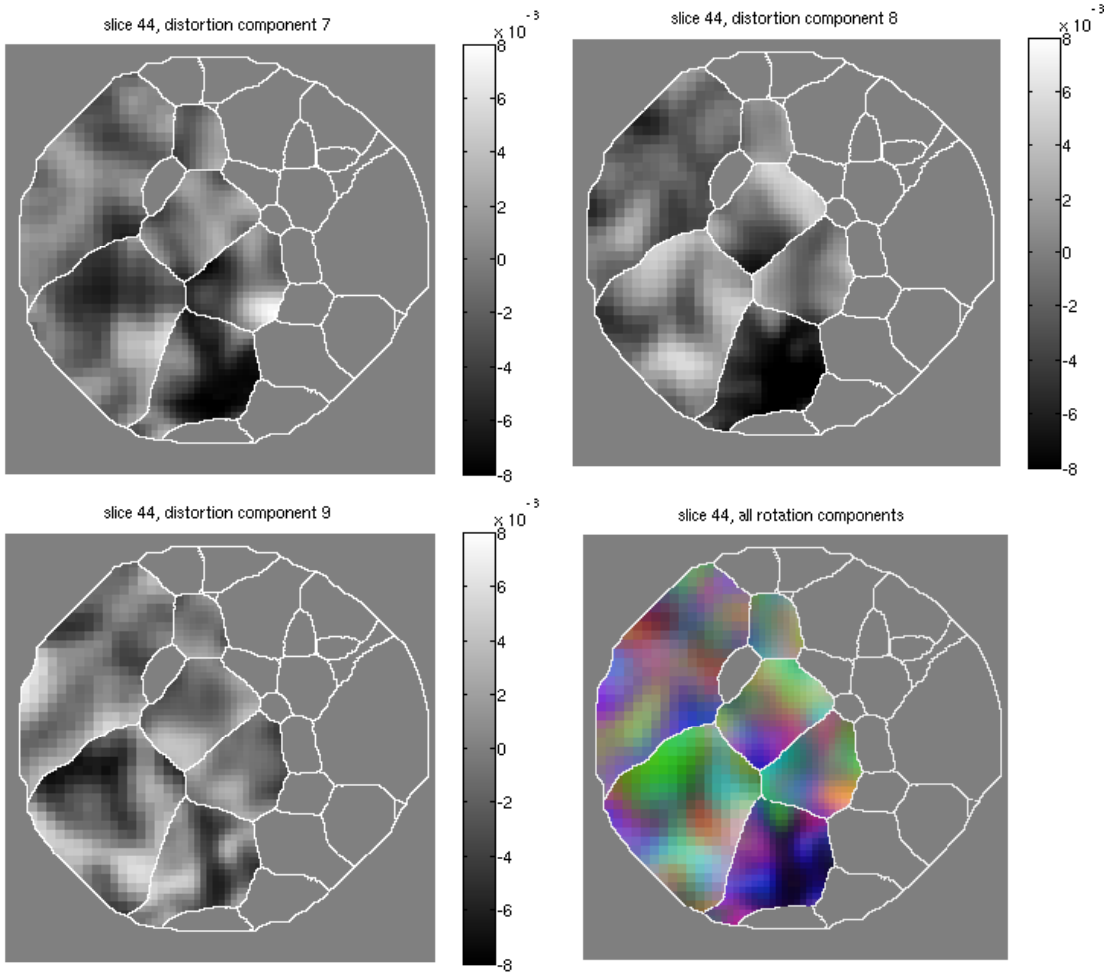

Fig. 8. Subgrain misorientation calculated from the in-line detector scan. (a) R_x, (b) R-, (c) R-, (d) the three components represented as an RGB triple.

geometries may allow such lattice distortions to be determined more easily, and thus provide a means of validation (Ludwig 2010). Another approach could be the measurement of a sample in which a well known misorientation distribution has been introduced.

6.2 Perspectives for the HEMS beamline. The high energy materials science (HEMS) beamline at the new Petra III synchrotron radiation source in Hamburg will feature an instrument dedicated to grain tracking experiments, which will be well suited to this type of investigation. An overview of this instrument is shown in figure 11. The instrument is designed to offer very good mechanical precision and stability, whilst being flexible and facilitating experiments using combinations of complementary techniques. The instrument will feature the 3D detector system developed by Risø, allowing two high resolution images at different working distances to be acquired simultaneously (Olsen et al 2008). Additionally, there will be the possibility to position detectors much further from the sample to perform high resolution 3D XRD type measurements.

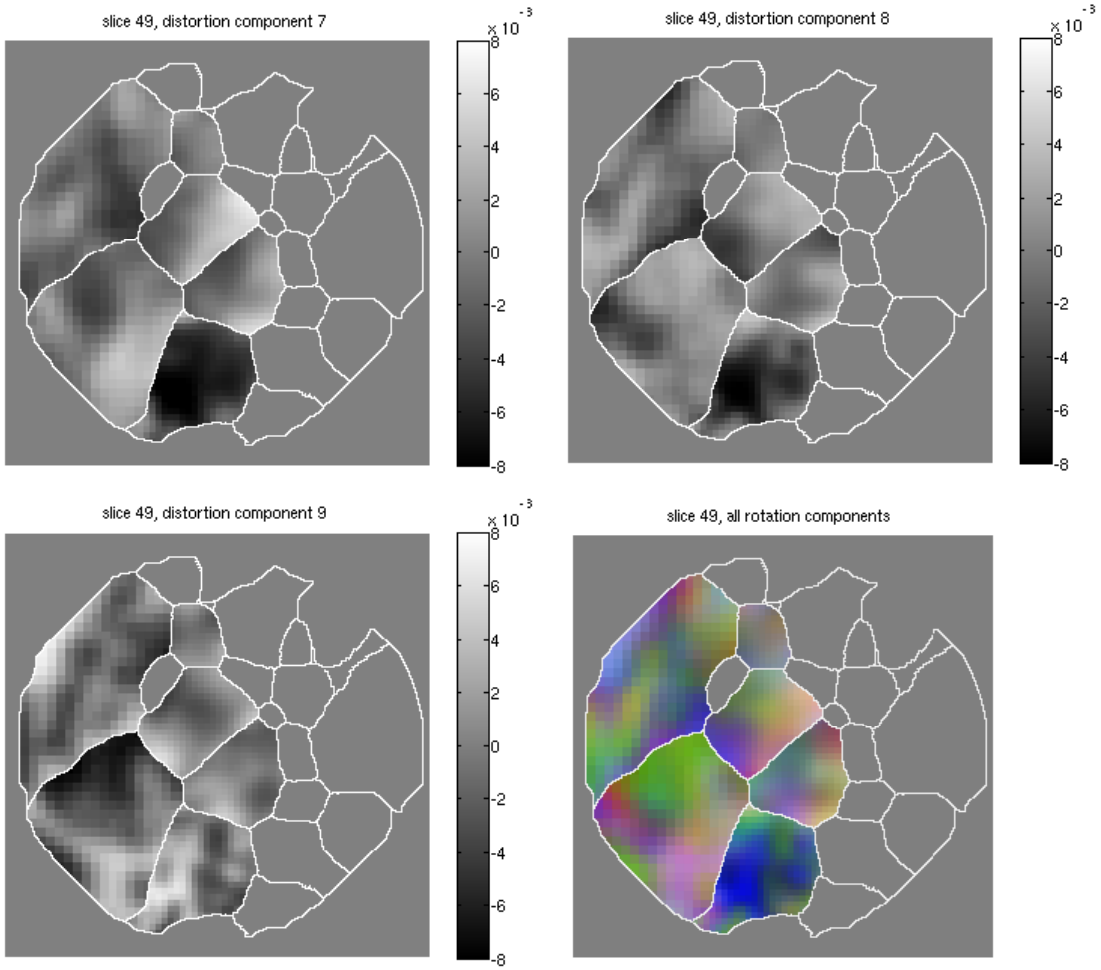

Fig. 9. Subgrain misorientation calculated from the scan with offset detctor and longer working distance. (a) R_x, (b) R-, (c) R-, (d) the three components represented as an RGB triple.

7.

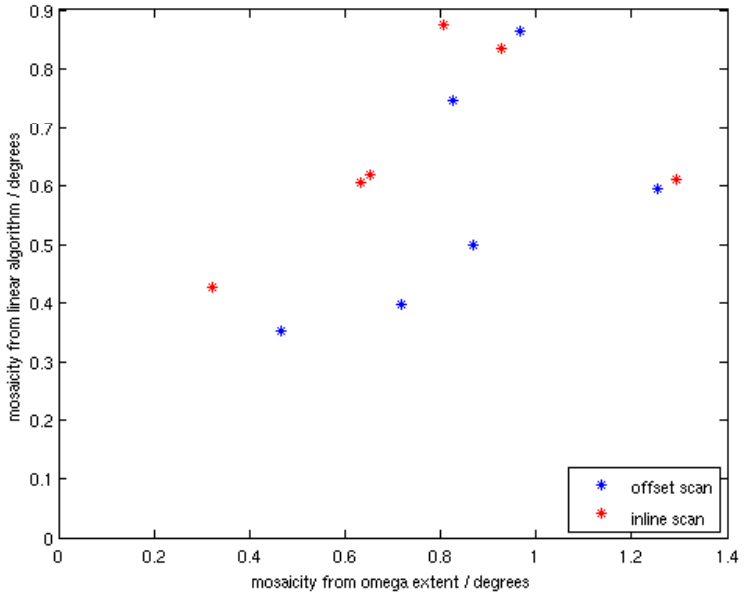

Fig. 10. Correlation between mosaicity determined from the ω extent of diffraction spots (x) and mosaicity determined from the linear algorithm (y).

CONCLUSIONS

The experimental techniques discussed in this paper provide a possible route to the in-situ, 3D study of plastic deformation in polycrystalline materials by the extension of the standard DCT analysis. Further development of the technique is required, as well as validation of the results obtained. If ultimately successful, this technique has great potential for the study of polycrystalline plasticity. Through a better understanding of the relationship between grain shape and misorientation distribution, and the diffraction spot observed, it may also lead to better algorithms for the reconstruction of grain maps.

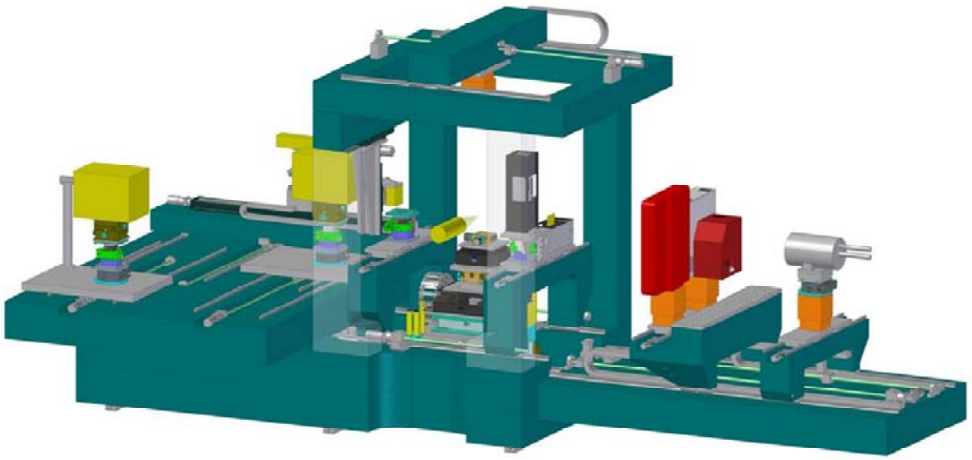

Fig 11. The grain mapping instrument that will be constructed at the HEMS beamline, Petra III.

REFERENCES

Dingley, D.J. and Randle, V. (1992). Review: Microtexture determination by electron back-scatter diffraction. J. Mat. Sci. 27, 4545-4566.

Fonseca, J., Oliver E.C., Bate P.S. and Withers, P.J. (2006). Evolution of intergranular stresses during in situ straining of IF steel with different grain sizes. Mat. Sci. Eng. A 437, 26-32.

Jakobsen, B., Poulsen, H.F, Lienert, U. and Pantleon, W. (2007). Direct determination of elastic strains and dislocation densities in individual subgrains in deformation structures. Acta Mater. 55, 3421-3430.

Johnson, G., King, A., Honnicke, M.G., Marrow, J. and Ludwig, W. (2008). X-ray diffraction contrast tomography: a novel technique for three dimensional grain mapping of polycrystals. II. The combined case. J. Appl. Cryst. 41, 310-318

Labiche, J.-C., Mathon, O., Pascarelli, S., Newton, M.A., Ferre, G.G., Curfs, C., Vaughan, G., Homs, A. and Carreiras, D.F. (2007). The fast readout low noise camera as a versatile x-ray detector for time resolved dispersive extended x-ray absorption fine structure and diffraction studies of dynamic problems in materials science, chemistry, and catalysis. Rev. Sci. Instrum. 78, 091301.

Lang, A.R. and Makepeace, A.P.W. (1996). Reticulography: a simple and sensitive technique for mapping misorientations in single crystals. J. Synchrotron Rad. 3, 313-315.

Larson, B.C., Yang, W., Ice, G.E., Budai, J.D. and Tischler, J.Z. (2002). Three-dimensional X-ray structural microscopy with submicrometre resolution. Nature 415, 887-890.

Ludwig, W., Cloetens, P., Härtwig, J., Baruchel, J., Hamelin, B. and Bastie, P. (2001). Three-dimensional imaging of crystal defects by 'topo-tomography'. J. Appl. Cryst. 34, 602-607.

Ludwig, W., Schmidt, S., Lauridsen, E.M. and Poulsen, H.F. (2008) X-ray diffraction contrast tomography: a novel technique for three dimensional grain mapping of polycrystals. I. Direct beam case. J. Appl. Cryst. 41, 302-309.

Ludwig, W., Reischig, P., King, A., Herbig, M., Lauridsen, E.M., Johnson, G., Marrow, T.J. and Buffière, J.Y. (2009). Three-dimensional grain mapping by x-ray diffraction contrast tomography and the use of Friedel pairs in diffraction data analysis. Rev. Sci. Instrum. 80, 033905.

Ludwig, W. (2010). To be presented in this conference.

Olsen, U.L., Schmidt, S. and Poulsen, H.F. (2008). A high-spatial-resolution three-dimensional detector array for 30-200 keV X-rays based on structured scintillators. J. Synchrotron Rad. 15, 363-370.

Poulsen, H.F. (2004). Three-Dimensional X-Ray Diffraction Microscopy: Mapping Polycrystals and Their Dynamics (Springer, Berlin)

Reischig, P. (2010). To be presented in this conference.

Sylwestrowicz, W. and Hall, E.O. (1951). The Deformation and Ageing of Mild Steel. Proc. Phys. Soc. B 64, 495-502.

West, S.S., Schmidt, S., Sørensen, H.O., Winther, G., Poulsen, H.F., Margulies, L., Grundlach, C. and Juul Jensen, D. (2009). Direct non-destructive observation of bulk nucleation in 30% deformed aluminium. Scripta Mater. 61, 875-878.

Wilkinson, A.J., Meaden, G. and Dingley, D.J. (2006). High resolution mapping of strains and rotations using electron backscatter diffraction. Mat. Sci. and Tech. 22, 1271-1278(8).

Wright, S.I. and Field, D.P. (1998) Recent studies of local texture and its influence on failure. Mat. Sci. Eng A 257, 165-170.